TUMOR SEGMENTATION FROM MAGNETIC RESONANCE IMAGING BY LEARNING VIA ONE-CLASS SUPPORT VECTOR MACHINE

Jianguo Zhang, Kai-Kuang Ma*, Meng Hwa Er

School of Electrical & Electronic Engineering
Nanyang Technological University, Singapore
Email: {ejgzhang, ekkma, emher}@ntu.edu.sg

Vincent Chong

National Cancer Center
Singapore General Hospital, Singapore
Email: gdrcfh@sgh.com.sg

ABSTRACT

In image segmentation, one challenge is how to deal with the non-linearity of real data distribution, which often makes segmentation methods need more human interactions and make unsatisfied segmentation results. In this paper, we formulate this research issue as a one-class learning problem from both theoretical and practical viewpoints with application on medical image segmentation. For that, a novel and user-friendly tumor segmentation method is proposed by exploring one-class *support vector machine* (SVM), which has the ability of learning the nonlinear distribution of the tumor data without using any prior knowledge. Extensive experimental results obtained from real patients' medical images clearly show that the proposed unsupervised one-class SVM segmentation method outperforms supervised two-class SVM segmentation method in terms of segmentation accuracy, speed and with less human intervention.

1. INTRODUCTION

Medical image segmentation plays an instrumental role in clinical diagnosis. An ideal medical image segmentation scheme should possess some preferred properties such as minimum user interaction, fast computation, and accurate and robust segmentation results [1][2]. The existing works on medical image segmentation have been focusing on X-ray, Magnetic Resonance Imaging (MRI), CT and ultrasound images, and they can be broadly classified into three methodologies: *region growing methods*, *shape-based methods*, and *statistical methods*.

Region growing methods [3] provide a simple way for segmentation. These methods require user to manually select a seed in an image followed by applying a region growing process. To reduce some unnecessary computations, a *region of interest* (ROI) can be further imposed. The major drawback of this method is that it requires a considerable amount of human intervention to specify the criteria for region growth and to select the seed candidates to achieve a satisfied segmentation result. Another drawback of this method is that it only works well for homogenous regions. *Shape-based methods* such as active contour [4][5] provide another school of approaches for medical image segmentation. But the disadvantages of these methods lie in the difficulty of selecting the optimal initial contour. Improper selection of the initial contour will results in unsatisfactory results. Moreover, the convergence speed is often very slow. Other sophisticated methods including *statistical methods* and *fuzzy logic approaches* [6] are introduced into this field recently. These methods usually define a
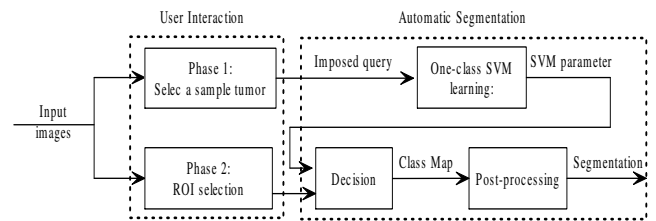

Fig. 1. The schematic diagram of the proposed tumor segmentation method based on one-class *support vector machine* (SVM).

specific parameterized distribution, and the major work is to estimate such predefined parameters. It means that such approaches have implicitly imposed some prior assumptions about the data distribution. Accordingly, their performance heavily depends on how well the assumed distribution is close to the real data distribution. They are only useful when the data distributions of different tissue classes are known in prior [7]. However, in real cases, especially in medical applications (e.g., MRI tumor segmentation), we usually have no prior knowledge about the data distribution. Thus automatic learning of these nonlinear distributions is desirable.

In this paper, we propose a novel and user-friendly tumor segmentation approach by exploring one-class SVM (see Fig. 1). In the proposed segmentation framework, the user is only required to feed one-class SVM classifier with a chosen image sample over a tumor area as the query for performing segmentation. Then, our approach can intelligently learn the nonlinear tumor data distribution without additional prior knowledge and optimally generate an accurate boundary of the tumor region. The final segmentation result can be obtained after region analysis. Note that SVM can generalize well in higher-dimensional spaces, and feature extraction can be automatically performed during the training stage of SVM [8]. No specific feature extraction approach is required.

2. ONE-CLASS, TWO-CLASS, AND MULTI-CLASS SVM FOR IMAGE SEGMENTATIONS

Statistical segmentation methods perform the task of classifying and grouping the image pixels into unified regions according to a certain criteria. The key task is usually performed by some selected pattern classifiers plus some necessary post-processing techniques such as morphological filtering. In tumor segmentation, the focus is to separate the tumor data ('positive' pattern) from the
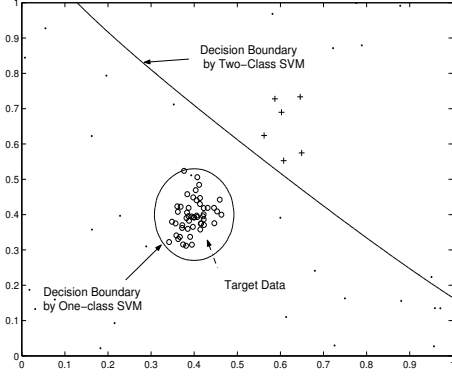
Fig. 2. Undesirable classification result by two-class SVM. Legend '○' indicates the target samples for training and legend '+' indicates the relevant non-target data for training. Two-class SVM is trained on the samples indicated by '○' and '+'. One-class SVM is trained only on the samples indicated by '○'.

non-tumor data ('negative' pattern). The following discussion is focused on segmentation based on one-class and two-class, which can be easily generalized to the case of multi-class classification.

In two-class classification, the data from two classes are available. The decision boundary is 'supported' from both sides. Most two-class classifiers assume more or less equally-balanced data classes and thus do not work well when one class is severely under-sampled or even completely absent. An illustration of undesirable classification result reached by two-class SVM is given in Fig. 2. In this figure, the decision boundary generated by two-class SVM is based on the training samples indicated by legends '○' and '+'. It is obvious that the two-class SVM has misclassified a large part of non-target data (indicated by legend '.') into the target data, which is unacceptable. To achieve a satisfied tumor segmentation result by using two-class classification, user needs to know the number of classes and the distributions of tumor data and non-tumor data in order to achieve representative and balanced data samples. The requirement is impractical and often impossible to meet. These disadvantages make the conventional segmentation systems not so useful.

On the other hand, one-class SVM performs well in separating the target data (tumor region in this case) from others – see the circle around the target data as the decision boundary produced by one-class SVM. Therefore, from both practical and theoretical viewpoints, we argue that the tumor segmentation issue could be formulated as a one-class learning problem and accordingly propose a new segmentation approach based on one-class SVM.

3. MATHEMATICAL FOUNDATION OF ONE-CLASS SVM

One-class SVM constructs a classifier only from a set of labelled positive patterns, called *positive training samples* [9]. Suppose that the user has the following training data set:

$$\chi = \{\mathbf{x}_i | \ i = 1, 2, 3, \ldots, l\} \qquad (1)$$

where $\mathbf{x}_i$ is the ith observation and $l \in N$ is the number of observations. Consider there is a feature map, which maps the training data into a higher-dimensional inner-product space, called *feature*

space F. That is, $\Phi : \chi \to F$. Thus the image of a training sample $\mathbf{x}_i$ in χ is represented as $\Phi(\mathbf{x}_i)$ in F. We want to compute a function f which takes the value +1 for the tumor data (positive samples) and -1 for the non-tumor data (negative samples) outside the tumor region. In the feature space, our strategy is to separate the data from the origin with the maximum margin. Therefore we only consider the tumor data, and the objective function is formulated as follows:

$$\min_{\mathbf{W} \in F, \boldsymbol{\eta} \in R^t, b \in R} \frac{1}{2} \mathbf{W}^T \mathbf{W} + \frac{1}{vl} \sum_i \eta_i - b \qquad (2)$$

$$s.t. \ \mathbf{W} \cdot \Phi(\mathbf{x}_i) \geq b - \eta_i, \ \eta_i \geq 0$$

where $\mathbf{W}$ is the normal vector of the hyperplane which represents the decision boundary. b represents the threshold of function f, η_i is the slack variable, which is penalized in the objective function. The regularization term v is a user-defined parameter, which controls the trade-off and indicates the fraction of samples that should be accepted by the description. We want to compute the parameters $\mathbf{W}$ and b, which give the minimization of the objective function (Eq. (2)). Therefore, we introduce the positive Lagrange multipliers, α_i, and β_i (for $i = 1, 2, \cdots, l$), one for each of the inequality constrains in (2). This gives the following Lagrange form:

$$L(\mathbf{W}, \boldsymbol{\eta}, b, \boldsymbol{\alpha}, \boldsymbol{\beta}) = \frac{1}{2} \mathbf{W}^T \mathbf{W} + \frac{1}{vl} \sum_i \eta_i - b - \sum_i \beta_i \eta_i$$
$$- \sum_i \alpha_i (\mathbf{W} \cdot \Phi(\mathbf{x}_i) - b + \eta_i) \qquad (3)$$

where $\boldsymbol{\eta}, \boldsymbol{\alpha}$, and $\boldsymbol{\beta}$ are one-column vectors representing $[\eta_i], [\alpha_i]$, and $[\beta_i]$, respectively. To minimize $L(\mathbf{W}, \boldsymbol{\eta}, b, \boldsymbol{\alpha}, \boldsymbol{\beta})$, we let its gradient, with respect to $\mathbf{W}$, b, and η_i, individually, equal to zero. That is,

$$\frac{\partial L}{\partial \mathbf{W}} = \mathbf{W} - \sum_i \alpha_i \Phi(\mathbf{x}_i) = 0 \Longrightarrow \mathbf{W} = \sum_i \alpha_i \Phi(\mathbf{x}_i) \quad (4)$$

$$\frac{\partial L}{\partial b} = -1 + \sum_i \alpha_i = 0 \Longrightarrow \sum_i \alpha_i = 1 \qquad (5)$$

$$\frac{\partial L}{\partial \eta_i} = \frac{1}{vl} + \alpha_i - \beta_i = 0 \Longrightarrow a_i = \frac{1}{vl} - \beta_i \leq \frac{1}{vl} \quad (6)$$

Substituting (4)-(6) into (3), we obtain the following dual problem:

$$\min_{\boldsymbol{\alpha}} \frac{1}{2} \sum_{i,j} \alpha_i \alpha_j k(\mathbf{x}_i, \mathbf{x}_j)$$
$$s.t. \ 0 \leq \alpha_i \leq \frac{1}{vl}, \ \sum_i \alpha_i = 1 \qquad (7)$$

where $k(\mathbf{x}_i, \mathbf{x}_j)$ represents the inner product of $\Phi(\mathbf{x}_i)$ and $\Phi(\mathbf{x}_j)$; that is, $k(\mathbf{x}_i, \mathbf{x}_j) = \Phi(\mathbf{x}_i) \cdot \Phi(\mathbf{x}_j)$

Eq. (7) can be further written in a more compact matrix form:

$$\min_{\boldsymbol{\alpha}} \frac{1}{2} \boldsymbol{\alpha}^T \mathbf{Q} \boldsymbol{\alpha}$$
$$s.t. \ 0 \leq \alpha_i \leq \frac{1}{vl}, \ \mathbf{e}^T \alpha = 1 \qquad (8)$$

where $\mathbf{Q}_{i,j} = k(\mathbf{x}_i, \mathbf{x}_j)$ and $\mathbf{e}$ is an unit vector of length N. Note that the dual problem in (8) presents a quadratic form, and its minimization can be solved by using the well-known quadratic programming (QP) optimization method. The optimal value of $\boldsymbol{\alpha}$ corresponds to the minimum of the objective function. Those objects with weight $\alpha_i > 0$ are required in the final description of the data set. They are commonly called *support vectors* in machine learning research.

The optimal value of the parameter b can be computed via the following equation:

$$b = \sum_j \alpha_j k(\mathbf{x}_j, \mathbf{x}_i) \tag{9}$$

where $\mathbf{x}_i$ corresponds to any one of the support vectors. Once the optimal values of the parameters are obtained, we can classify the tumor data according to the following decision function:

$$f(\mathbf{x}) = sgn\left(\sum_i \alpha_i k(\mathbf{x}_i, \mathbf{x}) - b\right) \tag{10}$$

The data corresponding to $f(\mathbf{x}) \geq 0$ are determined as the tumor data candidates. Otherwise, they are regarded as the non-tumor candidates.

4. KERNEL-BASED FLEXIBLE DESCRIPTION

The learning ability of one-class SVM originates from the 'kernel trick' introduced by Vapnik [9]. This 'trick' is accomplished by different choices of kernel function $k(\mathbf{x}, \mathbf{y})$ introduced in Section 3. Note that in the formulation of one-class SVM, the mapping Φ is only defined implicitly by the kernel $k(\mathbf{x}, \mathbf{y})$. Thus, we do not need to give an explicit mapping but to define a kernel instead. Commonly used kernels are summarized as follows:

- Radial basis function (RBF): $k(\mathbf{x}, \mathbf{y}) = \exp\left(\frac{-\|\mathbf{x}-\mathbf{y}\|^2}{\sigma}\right)$
- Polynomial kernel: $k(\mathbf{x}, \mathbf{y}) = (\mathbf{x} \cdot \mathbf{y})^n$
- Tangent hyperbolic kernel: $k(\mathbf{x}, \mathbf{y}) = \tanh(\mathbf{x} \cdot \mathbf{y} + \Theta)$

where σ, n, and Θ are the parameters of RBF kernel, polynomial kernel, and tangent hyperbolic kernel, respectively. It has been pointed out that these kernels are not equally useful. Among them, the preferable choice is the RBF kernel [9]. With the 'kernel trick', one-class SVM can deal with nonlinear multi-mode data distribution.

A toy experiment is conducted to demonstrate the learning ability of one-class SVM. The training data are jointly sampled from two 2-D normal distributions. In this section, one-class SVM is investigated in two cases: *linear* and *nonlinear*. In the linear case, $k(\mathbf{x}, \mathbf{y})$ equals to the inner product of the original data samples; i.e., $k(\mathbf{x}, \mathbf{y}) = \mathbf{x} \cdot \mathbf{y}$. One-class SVM directly performs the classification task in the input space without mapping the data to a higher-dimensional space. The learning ability of linear one-class SVM is demonstrated in Figs. 3(a)-(b). From this figure, we can see that it attempts to put a circle boundary in the 2-D space to include most of the positive samples, while leaving some out of the boundary. Furthermore, the boundary also includes an undesirable and superfluous region in the input space (see Fig. 3(a)). This is due to the fact that the hypersphere (for higher-dimensional input data) is a very rigid model, not flexible enough to give an accurate boundary of the data set.

For the nonlinear case, if we map the data to a new space by using the 'kernel trick', we might obtain a better fit around the actual data set's boundary. A possibly demonstration of the learning ability of one-class SVM using RBF kernel is performed on the same data set (see Figs. 3(c)-(d)). After learning, it can be clearly seen that the one-class SVM can capture the data distribution fairly well and intelligently produce a flexible boundary containing most of the training examples. Also the 3-D decision surface as shown in Fig. 3 clearly confirms a good match with the true data distribution. The 'kernel trick' gives the active learning ability to one-class SVM, which can solve the nonlinearity of data distribution for tumor segmentation of MRI as mentioned in Section 2.
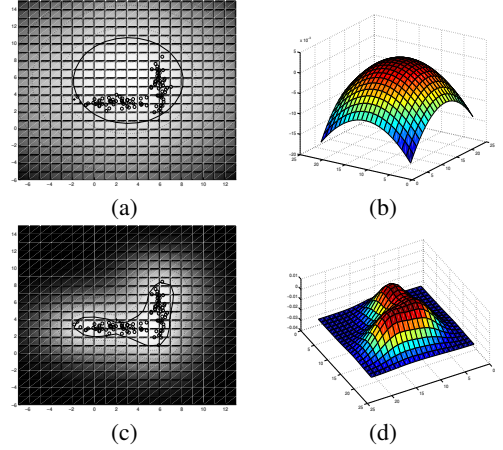
Fig. 3. Resulting flexible description of one-class SVM on the training data generated from two Gaussian distributions. (a) Decision boundary generated by *linear* one-class SVM via the inner product; (b) The corresponding 3-D decision surface of (a); (c) Decision boundary generated by *nonlinear* one-class SVM via the RBF kernel function; (d) The corresponding 3-D decision surface of (c).

5. SEGMENTATION MAP POST-PROCESSING

Any classification method could yield classification errors. In our proposed method, the mis-classified pixels usually take the form of isolated speckles scattered across the entire classification map as shown in Fig. 4(b). To remove these speckles, a morphological filter including dilation and erosion operations is applied as the post-processing technique — merging the connected regions while removing some isolated non-tumor regions. The eight-wise connected components operation is used in the refinement of tumor segmentation [7]. The effectiveness of this operation is demonstrated in Fig. 4(c). We can clearly see that the speckle noises have been removed.
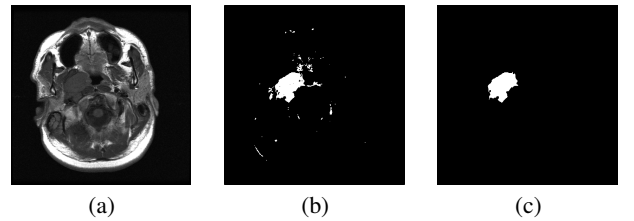
Fig. 4. An illustration of the role and effectiveness of segmentation map post-processing. (a) The original image; (b) The initial tumor segmentation map; (c) Post-processing result.

6. EXPERIMENTAL RESULTS

6.1. Comparison with the ground truth

To verify the effectiveness of the proposed segmentation method, several supervised segmentation experiments are performed on a

set of test images. These test images are nasopharyngeal carcinoma slices (Fig. 5) from MRI system acquired from real patients. They are scanned from the top of the patients' brain and downward. Each patient's MRI anatomic slice contains two feature images: one is imaged by MRI system without adding the contrast agent to the patient (Fig. 5a) and the other is obtained after adding the contrast agent (Fig. 5b). Both of the two feature images are used in our tumor segmentation task. The gray levels of the tumor sample selected by the user as a query are directly fed into one-class SVM to train its parameters. The average processing time of tumor segmentation is around 6.85s for one anatomic slice containing two feature images of size 512×512 each (implemented in MATLAB on a Pentium III 2.4 MHz PC). To save the computation time, user has an option to impose a ROI rather than the entire image slice at the graphical user interface stage.

In our experiment, a Gaussian RBF kernel is chosen as the machine kernel function as mentioned in Section 4. After learning, the approach classifies the medical data according to the decision boundary specified by (10). Post-processing morphological filtering is then performed on the obtained binary classification map. The tumor segmentation results are compared with the respective 'ground truth' tumor segmentations that were manually segmented by radiologist. Quantitative measurement of segmentation accuracy are calculated in terms of *true positive* (TP) with respect to the ground truth.

Let GT and Ω denote the set of tumor pixels of the ground truth and the set of the tumor pixels of our segmentation results, respectively. The TP can be defined as follows:

$$TP = \{x(i,j) \mid x \in GT, x \in \Omega\} = GT \cap \Omega \qquad (11)$$

where $x(i,j)$ represents intensity of the medical image pixel at the location (i,j). To give an objective evaluation of our segmentation results with respect to the ground truth, the following commonly used criteria is adopted [1] :

$$MP = \frac{\#TP}{\#GT} \qquad (12)$$

where symbol # denotes the *cardinality* of a set. Therefore, MP is the percentage of correct match between our segmentation results and the ground truth.

Based on the difference between GT and Ω, *false positive* (FP) and *false negative* (FN) are further defined as follows:

$$FP = \{x(i,j) \mid x \notin GT, x \in \Omega\} = \overline{GT} \cap \Omega \qquad (13)$$

$$FN = \{x(i,j) \mid x \in GT, x \notin \Omega\} = GT \cap \overline{\Omega} \qquad (14)$$

In our experiments, the comparison results in terms of $\#TP$, $\#FP$, $\#FN$, $\#GT$, and MP are tabulated in Table 1. The higher the MP value, the larger $\#TP$ (i.e., correct tumor segmentation) contained in the results. From Table 1, we can see that the segmentation results achieve a high percentage of correct match to the ground truth. Most of the MP values are around 90%. Fig. 5 shows some examples of our segmentation results versus their respective ground truth to give an visual comparison. The segmentation results are promising and are acceptable by radiologists in this field.

6.2. One-class SVM versus two-class SVM

One of the advantages of this one-class SVM-based approach is that human interactions have been greatly reduced, while yielding

**Table 1**. One-class SVM based tumor segmentation results versus the ground truth.

No.	$\#TP$	$\#FP$	$\#FN$	$\#GT$	MP
1	4192	74	522	4714	0.89
2	3465	302	273	3738	0.93
3	3696	1326	348	4044	0.91
4	2899	445	189	3088	0.94
5	1715	909	109	1824	0.94
6	1176	709	111	1287	0.91
7	1113	497	135	1248	0.88
8	5336	2244	465	5801	0.92
9	5565	1242	975	6540	0.86
10	4568	1553	739	5307	0.86
11	6597	628	1060	7657	0.86

very good segmentation results compared to other supervised two-class or multi-class based segmentation methods. It has reduced the risk of producing unsatisfied segmentation results due to unbalanced data cluster sizes – the tumor region versus the non-tumor region. The corresponding principle has been analyzed in Section 2. We here experimentally make a comparison of the proposed method with two-class SVM-based segmentation scheme. The reason why we selected two-class SVM as the representative two-class classifier is that many studies have indicated that two-class SVM outperforms other conventional two-class classifiers in most cases [10][11]. To have a fair comparison, we only replace the algorithm of one-class SVM with two-class SVM while keeping other processing steps unchanged. For two-class SVM, in order to obtain satisfied segmentation results, time-consuming human interactions are required to select the representative data samples of the tumor and the non-tumor tissues, respectively. Table 2 tabulates the segmentation results using supervised two-class SVM segmentation technique. Compared with Table 1, it is worth to note that two-class SVM produces less FPs than one-class SVM. This observation is justified because two-class SVM utilizes the separation information provided by the tumor data and the non-tumor data. Thus, after training, the classifier has built up the discrimination capability to differentiate the tumor data and the non-tumor data. From this table, we can see that the tumor segmentation results by one-class SVM are overall better than those by the *supervised* two-class SVM in terms of the values of MP. Moreover, our proposed method requires less human interactions. Thus, it is user-friendly and practical in clinic use.

7. CONCLUSIONS

Segmentation or extraction of a concerned region from medical images is a challenging yet unsolved task due to large variations and complexity of the human anatomy and pathological lesions. Currently, there are no universally accepted methods on quantifying tumor size in clinical practice [1]. In this paper, the proposed approach based on one-class SVM has demonstrated great potential and usefulness in MRI tumor segmentation.

The proposed segmentation approach has the ability of learning nonlinear distribution of medical data without prior knowledge. Experimental results in this paper have shown that the segmentation results of the proposed approach are better than the supervised two-class SVM learning algorithm in terms of the values
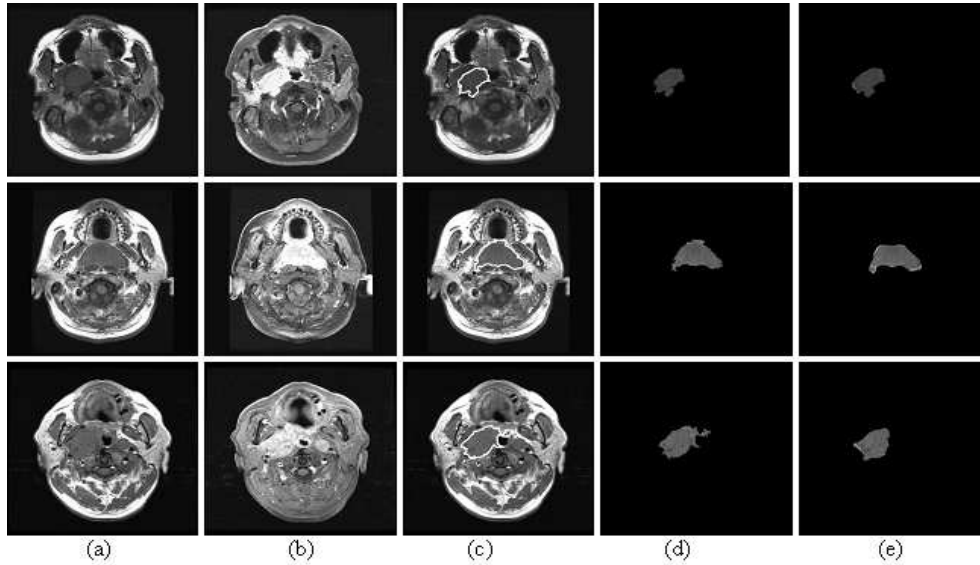
Fig. 5. Examples of tumor segmentation results from three patients versus the ground-truth segments (row-wise, from top to bottom, corresponding to different patient's MRI slices, respectively). (a)-(b) The original nasopharyngeal carcinoma MRI feature images, before and after adding the contrast agent, respectively; (c) The tumor boundary, as shown in white contour, has been detected by using our proposed one-class SVM method; (d) Segmented tumor area (same as (c), but for ease of visualization); (e) The ground truth segments.

.

Table 2. Two-class SVM tumor segmentation results with respect to the ground truth

No.	#TP	#FP	#FN	#GT	MP
1	4110	71	954	4714	0.87
2	3425	198	313	3738	0.90
3	3353	1067	691	4044	0.78
4	2512	118	576	3088	0.75
5	1711	390	113	1824	0.83
6	1193	299	94	1287	0.93
7	893	248	355	1248	0.72
8	3899	286	1194	5081	0.77
9	5433	980	1107	6540	0.83
10	4778	1882	529	5307	0.90
11	6208	601	1449	7657	0.81

of MP (i.e., correct matching). Furthermore, it only requires the user to feed the algorithm with a 'query' tumor sample. Hence it reduces user interactions and increases the feasibility of the proposed method. To conclude, the proposed scheme is a novel and user-friendly tumor segmentation method from the practical viewpoint.

Acknowledgment

8. REFERENCES

[1] M.C. Clark, L.O. Hall, D.B. Goldgof, R. Velthuizen, F.R. Murtagh, and M.S. Silbiger, "Automatic tumor segmentation using knowledge-based techniques," *IEEE Trans. on Medical Imaging*, vol. 17, no. 2, pp. 238–251, April 1998.

[2] S.D. Olabarriaga and A.W.M. Smeulders, "Interaction in the segmentation in medical images: A survey," *Medical Image Analysis*, vol. 5, no. 2, pp. 127–142, June 2001.

[3] M. Lenvine and S. Shaheen, "A modular computer vision system for image segmentation," *IEEE Trans. on Pattern Analysis and Machine Intelligence*, vol. 3, no. 5, pp. 540–557, May 1981.

[4] A. Yezzi, S. Kichenassamy, A. Kumar, P. J. Olver, and A. Tannenbaum, "A geometric snake model for segmentation of medical imagery," *IEEE Trans. on Medical Imaging*, vol. 16, no. 2, pp. 199–209, Feb. 1997.

[5] T. McInerney and D. Terzopolous, "Deformable models in medical image analysis: A survey," *Medical Image Analysis*, vol. 1, no. 2, pp. 91–108, June 1996.

[6] D. L. Pham and J. L. Prince, "An adaptive fuzzy segmentation algorithm for three-dimensional magnetic resonance image," *Information Processing in Medical Imaging, Lecture Notes in Computer Science*, vol. 1613, pp. 140–153, 1999.

[7] L. Clarke, R. Velthuizen, M. Camacho, J. Heine, M. Vaydianathan, L. Hall, R. Thatcher, and M. Silbiger, "MRI segmentation: methods and applications," *Magnetic Resonance Imaging*, vol. 13, no. 3, pp. 343–368, April 1995.

[8] K. I. Kim, K. Jung, S. H. Park, and H. J. Kim, "Support vector machines for texture classification," *IEEE Trans. on Pattern Analysis and Machine Intelligence*, vol. 24, no. 11, pp. 1542–1550, Nov. 2002.

[9] B. Schölkopf and A. J. Smola, *Learning with Kernels Support Vector Machines, Regularization, Optimization and Beyond*, MIT Press: Cambridge, M.A., 2002.

[10] G. Rätsch, T. Onoda, and K.-R. Müller, "Soft margins for AdaBoost," *Machine Learning*, vol. 42, no. 3, pp. 287–320, March 2001.

[11] K. Chan, T.-W. Lee, P. A. Sample, M. Goldbaum, and R. N. Weinreb, "Comparison of machine learning and traditional classifiers in glaucoma diagnosis," *IEEE Trans. on Biomedical Engineering*, vol. 49, no. 9, pp. 963–974, Sept. 2002.